

# CASTER: A Computer-Vision-Assisted Wireless Channel Simulator for Gesture Recognition

Zhenyu Ren, Guoliang Li, Chenqing Ji, Chao Yu, Shuai Wang, Rui Wang

**Abstract**—In this paper, a computer-vision-assisted simulation method is proposed to address the issue of training dataset acquisition for wireless hand gesture recognition. In the existing literature, in order to classify gestures via the wireless channel estimation, massive training samples should be measured in a consistent environment, consuming significant efforts. In the proposed CASTER<sup>1</sup> simulator, however, the training dataset can be simulated via existing videos. Particularly, a gesture is represented by a sequence of snapshots, and the channel impulse response of each snapshot is calculated via tracing the rays scattered off a primitive-based hand model. Moreover, CASTER simulator relies on the existing videos to extract the motion data of gestures. Thus, the massive measurements of wireless channel can be eliminated. The experiments demonstrate a 90.8% average classification accuracy of simulation-to-reality inference.

## I. INTRODUCTION

Sensing is becoming one of the core features of the next-generation wireless systems. There have been a significant number of works on the machine-learning-based human motion recognition (HMR) via channel state information (CSI) or passive sensing. In most of these works, a significant number of labelled wireless signals should be collected and processed for the training of motion recognition model, which might be infeasible in many applications. In this paper, we would like to show that it is possible to generate the above training dataset for hand gesture recognition via channel simulation, instead of real measurement.

In fact, there have been a number of works on the extension of sophisticated communication channel models, such that the effects of sensing target on the channel impulse response are incorporated. Hence, the channel simulation based on these models might be used for motion recognition. For instance, the Data Driven Hybrid Channel (DAHC) model of IEEE 802.11bf specification [1], [2] divided wireless channel into two parts: the target-unrelated components and the target-related components. The existing methods of communication channel modelling can be applied on the former; whereas, the primitive-based human body model [3] was utilized to compute the latter. Similar channel model was also used in [4] for the optimization of communication and sensing performance. The *WiGig Tools* [5], developed by National Institute of Standards and Technology (NIST), enriched existing quasi-deterministic channel ray-tracers with supplementary target-related rays (T-Rays). Moreover, the methods for simulating radar echo signals off the human body were proposed in [6], [7]. All the above works relied on the primitive-based

human body model [3], [8], where the hands were modelled as ellipsoids. These methods cannot model different hand gestures.

In machine learning, diversified training samples are usually required to improve the robustness of performance. Depth cameras and wearable sensors were used in [6], [7] to obtain sufficient body motion data for channel simulation. Nevertheless, there is no study on the capture of hand gestures for channel simulation. Moreover, it is unknown if conventional monocular cameras, instead of depth cameras, could obtain the motion data with adequate accuracy in the applications of wireless human motion recognition. In addition, utilizing monocular video simulation offers advantages such as lower cost and convenience, enabling the use of a wide range of hand gesture videos from online sources or the simulation of arbitrarily customized actions for channel simulation.

In this paper, we would like to shed some lights on the above three issues by proposing a computer-vision-assisted wireless channel simulator, namely CASTER, for hand gesture recognition. The proposed CASTER simulator is composed of channel generator and video gesture catcher. In the channel generator, the target hand is modelled with 21 primitives, and the channel impulse response is calculated by tracing the rays scattered off all the primitives. Based on the hand model, a gesture is represented by a sequence of snapshots, and the channel impulse responses for all the snapshots can be obtained. In the video gesture catcher, trajectories of 21 primitives in one gesture can be captured from videos of conventional monocular camera. Thus, the catcher provides an efficient way to retrieve motion data for the channel generator. In order to demonstrate the high fidelity of the proposed CASTER simulator, we use the simulated channel impulse responses to train a gesture classification model, and test the classification performance on the measured passive sensing dataset. It is shown that a 90.8% average classification accuracy for such simulation-to-reality inference can be achieved.

The remainder of this paper is organized as follows. The simulator framework is elaborated in Section II. The channel generator is presented in Section III, and the video gesture catcher is presented in Section IV. The evaluation of CASTER simulator, including simulation and measurement of datasets and the simulation-to-reality inference, is demonstrated in Section V. Finally, the conclusion is drawn in Section VI.

In this paper, we use the following notations: non-bold letters are used to denote scalar values, bold lowercase letters (e.g.,  $\mathbf{a}$ ) are used to denote column vectors, bold uppercase letters (e.g.,  $\mathbf{A}$ ) are used to denote matrices,  $|\mathbf{a}|$  and  $\mathbf{a}^T$  denote

<sup>1</sup>The code for the proposed CASTER simulator is available online at <https://github.com/rzy0901/testSpectrogram>

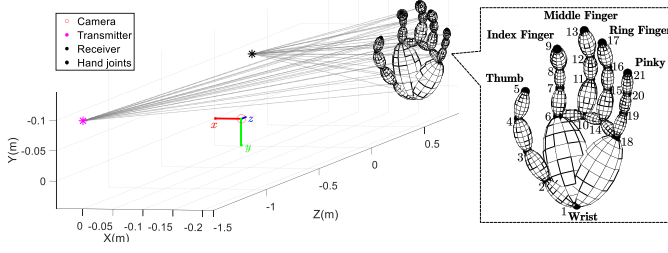


Fig. 1. Illustration of primitive-based hand model and channel simulation scenario.

the L2-norm and transpose of vector  $\mathbf{a}$ .

## II. SIMULATOR FRAMEWORK

The proposed CASTER simulator is developed with the primitive-based hand model. In order to extract high-fidelity channel impulse responses from existing videos, the CASTER simulator is composed of the channel generator and video gesture catcher. The former generates a sequence of channel impulse response snapshots given arbitrary hand gesture and arbitrary locations of the transmitter and receiver. The latter captures the parameters of real hand motions from existing videos as the former's input. As a result, the CASTER simulator is able to provide datasets for the training of hand gesture classification model without real channel measurement.

As depicted in Fig. 1, the locations of the transmitter, receiver and the target hand can be arbitrary in the channel generator. A gesture is represented as a sequence of snapshots, with an interval of  $\Delta t_s$  seconds. In each snapshot, the channel is assumed to be quasi-static, and the channel impulse response is calculated via the primitive-based method [3]. Particularly, the hand is modelled via 21 keypoints (joints) and 21 ellipsoids (primitives) connecting the keypoints. The non-line-of-sight (NLoS) channel components via the hand can be approximated by the 21 rays respectively scattered off the centers of all primitives. Hence, the channel impulse response of one snapshot can be obtained by aggregating all the rays from the transmitter to the receiver, including the line-of-sight (LoS) ray, the NLoS ones scattered off the target hand, and the others scattered at the environment.

Moreover, the proposed video gesture catcher first extracts the 3-dimensional (3D) coordinates of hand keypoints from each video frame in a local hand world coordination system via machine learning technique, converts the trajectories of the keypoints from the local hand world coordinate system to a global camera coordinate system, and then eliminates the fake hops and jitters of trajectories via low-pass filtering. Finally, since the interval between two video frames, denoted as  $\Delta t_v$ , is usually much larger than  $\Delta t_s$ , an interpolation is necessary to fill sufficient number of snapshots between two video frames.

## III. CHANNEL GENERATOR

Without loss of generality, the generation of channel impulse response for the  $t$ -th snapshot ( $\forall t$ ) is elaborated in this

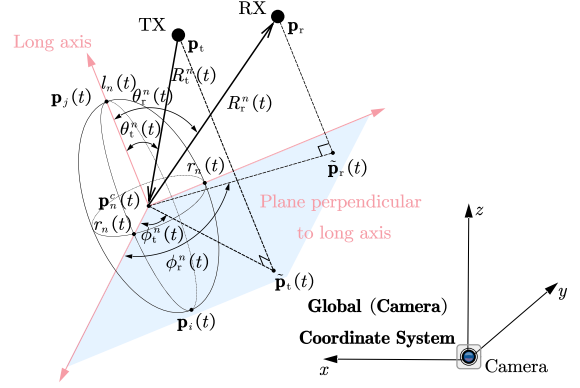


Fig. 2. Bistatic RCS estimation for the  $n$ -th primitive.

section. As shown in Fig. 1, the rays from the transmitter to the receiver can be categorized into two parts, target-unrelated components and target-related components. The former refers to the LoS ray and the NLoS rays scattered at the static environment; and the latter refer to the NLoS rays scattered off the target hand. Particularly, let  $h(\tau, t)$  and  $u(\tau, t)$  be the overall channel impulse response and target-related channel impulse response of the  $t$ -th snapshot,  $v(\tau)$  be time-invariant target-unrelated channel impulse response, we have

$$h(\tau, t) = u(\tau, t) + v(\tau), \quad (1)$$

where the generations of  $u(\tau, t)$  and  $v(\tau)$  are elaborated in the following parts respectively.

### A. Target-Related Channel Components

Let  $\mathbf{p}_t$  and  $\mathbf{p}_r$  be the coordinates of the transmitter and the receiver respectively,  $\mathbf{p}_i(t)$  and  $\mathbf{p}_j(t)$  be the coordinates of the two joints associated with the  $n$ -th primitive in the  $t$ -th snapshot ( $\forall n, t$ ). Hence, the center of the  $n$ -th primitive is  $\mathbf{p}_n^c(t) = [\mathbf{p}_i(t) + \mathbf{p}_j(t)]/2$ . As previously mentioned, each primitive is modelled as an ellipsoid, the length of the axis connecting the two joints is denoted as  $2l_n(t)$ , where

$$l_n(t) = |\mathbf{p}_i(t) - \mathbf{p}_j(t)|/2. \quad (2)$$

Moreover, the lengths of the other two axes are identical, denoted as  $2r_n(t)$ . Usually,  $r_n(t) < l_n(t)$ , and we choose  $r_n(t) = l_n(t)/2$ . Hence, we shall refer to the axis connecting the two joints as the long axis of the ellipsoid. As a remark note that the primitive size ( $r_n$  and  $l_n$ ) varies over time slightly due to the non-rigid nature of human motion.

Let  $R_t^n(t) = |\mathbf{p}_t - \mathbf{p}_n^c(t)|$  be the distance between the transmitter and the  $n$ -th primitive center,  $R_r^n(t) = |\mathbf{p}_r - \mathbf{p}_n^c(t)|$  be the distance between the receiver and the  $n$ -th primitive center,  $G_t^n(t)$  and  $G_r^n(t)$  be the transmit and receive antenna gains at the directions of incident ray  $\mathbf{p}_t - \mathbf{p}_n^c(t)$  and scattered ray  $\mathbf{p}_n^c(t) - \mathbf{p}_r$ ,  $\sigma_n(t)$  be the bistatic radar cross section (RCS) of the  $n$ -th primitive,  $c$  be the speed of light,  $f_c$  and  $\lambda$  be the carrier frequency and wavelength respectively. The response

$$\sigma_n(t) = \frac{4\pi r_n^4(t) l_n^2(t) [(1 + \cos \theta_t^n(t) \cos \theta_r^n(t)) \cos(\phi_r^n(t) - \phi_t^n(t)) + \sin \theta_t^n(t) \sin \theta_r^n(t)]^2}{[r_n^2(t) (\sin^2 \theta_t^n(t) + \sin^2 \theta_r^n(t) + 2 \sin \theta_t^n(t) \sin \theta_r^n(t) \cos(\phi_r^n(t) - \phi_t^n(t))) + l_n^2(t) (\cos \theta_t^n(t) + \cos \theta_r^n(t))^2]^2}. \quad (7)$$

of the path scattered off the  $n$ -th primitive can be expressed as

$$u_n(\tau, t) = \lambda \sqrt{\frac{\sigma_n(t) G_t^n(t) G_r^n(t)}{(4\pi)^3 (R_t^n(t) R_r^n(t))^2}} e^{-j\phi_n(t)} \delta(\tau - \tau_n(t)), \quad (3)$$

where  $\tau_n(t) = [R_t^n(t) + R_r^n(t)]/c$  and  $\phi_n(t) = 2\pi f_c \tau_n(t)$  measure the delay and phase shift.

Moreover, the calculation of the bistatic RCS  $\sigma_n(t)$  follows the method in [9], [10]. As depicted in Fig. 2, let  $\theta_t^n(t)$  and  $\theta_r^n(t)$  represent the incident and scattered elevation angles respectively,  $\phi_t^n(t)$  and  $\phi_r^n(t)$  represent the incident and scattered azimuth angles respectively,  $\mathbf{v}_n(t) = [\mathbf{p}_i(t) - \mathbf{p}_j(t)]/(2l_n(t))$  represent the normalized vector along the long axis, we have

$$\theta_t^n(t) = \arccos((\mathbf{p}_t^c(t) - \mathbf{p}_t)^T \mathbf{v}_n(t) / R_t^n(t)), \quad (4)$$

$$\theta_r^n(t) = \arccos((\mathbf{p}_r^c(t) - \mathbf{p}_r)^T \mathbf{v}_n(t) / R_r^n(t)), \quad (5)$$

and

$$|\phi_r^n(t) - \phi_t^n(t)| = \arccos\left(\frac{(\mathbf{p}_t^c(t) - \tilde{\mathbf{p}}_t(t))^T (\mathbf{p}_r^c(t) - \tilde{\mathbf{p}}_r(t))}{|\mathbf{p}_t^c(t) - \tilde{\mathbf{p}}_t(t)| |\mathbf{p}_r^c(t) - \tilde{\mathbf{p}}_r(t)|}\right), \quad (6)$$

where

$$\tilde{\mathbf{p}}_t(t) = \mathbf{p}_t - \mathbf{v}_n(t)(\mathbf{p}_t - \mathbf{p}_t^c(t))^T \mathbf{v}_n(t)$$

and

$$\tilde{\mathbf{p}}_r(t) = \mathbf{p}_r - \mathbf{v}_n(t)(\mathbf{p}_r - \mathbf{p}_r^c(t))^T \mathbf{v}_n(t)$$

denotes the projection of the transmitter and receivers' locations on the plane containing the center of the  $n$ -th ellipsoid and perpendicular to its long axis in the  $t$ -th snapshot. As a result, the bistatic RCS  $\sigma_n(t)$  of  $n$ -th ellipsoid in the  $t$ -th snapshot is given by (7).

Aggregating the NLoS rays scattered off all the primitives, the target-related channel impulse response can be written as

$$u(\tau, t) = \sum_{n=1}^{21} u_n(\tau, t). \quad (8)$$

### B. Target-Unrelated Channel Components

CASTER models the environment by  $K$  static scatters. Let the RCS, transmit and receive antenna gains and the distance of the  $k$ -th NLoS ray be  $\sigma_k$ ,  $G_t^k$ ,  $G_r^k$ ,  $R_t^k$ , and  $R_r^k$ , respectively. The NLoS components of target-unrelated channel impulse response can be written as

$$v_{\text{NLoS}}(\tau) = \sum_{k=1}^K \lambda \sqrt{\frac{\sigma_k G_t^k G_r^k}{(4\pi)^3 (R_t^k R_r^k)^2}} e^{-j\phi_k} \delta(\tau - \tau_k), \quad (9)$$

where  $\tau_k = (R_t^k + R_r^k)/c$  and  $\phi_k = 2\pi f_c \tau_k$ .

Moreover, let transmit and receive antenna gains at the direction of LoS path be  $G_{t, \text{LoS}}$  and  $G_{r, \text{LoS}}$ , distance between

transmitter and receiver be  $R_{\text{LoS}}$ , the LoS component of target-related channel is modeled via the following free space model:

$$v_{\text{LoS}}(\tau) = \frac{\sqrt{G_{t, \text{LoS}} G_{r, \text{LoS}}}}{4\pi R_{\text{LoS}}} e^{-j\phi_{\text{LoS}}} \delta(\tau - \tau_{\text{LoS}}), \quad (10)$$

where  $\tau_{\text{LoS}} = R_{\text{LoS}}/c$  and  $\phi_{\text{LoS}} = 2\pi f_c \tau_{\text{LoS}}$ . As a result, the target-unrelated channel impulse response can be written as

$$v(\tau) = v_{\text{LoS}}(\tau) + v_{\text{NLoS}}(\tau). \quad (11)$$

## IV. VIDEO GESTURE CATCHER

As mentioned in the previous section, a motion of the target hand is characterized by the trajectories of the 21 keypoints in a sequence of snapshots, denoted as  $\mathbf{p}_i(t)$ ,  $i = 1, 2, \dots, 21$ . We leverage the tool of *Mediapipe* [11] to extract the keypoint trajectories from videos, where two issues in the conversion are addressed in this section. The *Mediapipe* could localize the positions of the keypoints in each video frame. The positions are represented in the coordinate system with the origin at the hand center, namely hand world coordinate system. However, it is difficult to calculate the Doppler frequency with such coordinate system, as the hand center is moving. Hence, we first transfer the coordinates to a unified coordinate system by solving the Perspective-n-Point (PnP) problem [12], where the fake hops on the trajectories are smoothed. Moreover, because there are usually 30 video frames per second, which is not sufficient for estimating the Doppler frequencies of gesture. For example, the typical Doppler frequencies of gestures on the 60 GHz signals is around 400 Hz (assuming a maximum velocity of 2 meters per second), which requests 800 snapshots per second at least. Hence, interpolation are introduced such that the channel impulse response can be generated with a shorter interval.

### A. Conversion of Coordinate Systems

For the elaboration convenience, we first introduce the following three coordinate systems. The two-dimensional (2D) pixel coordinate system in the unit of pixels is used to identify the positions of hand keypoints in each video frame. The origin of the pixel coordinate system is usually at the upper left corner of each frame, as shown in Fig. 3. The three-dimensional (3D) hand world coordinate system in the unit of meters measures the positions of hand keypoints in the real world with respect to the hand center. Moreover, the 3D camera coordinate system in the unit of meters measures the positions of hand keypoints with respect to the static camera lens, which captures the videos. The *Mediapipe* is able to identify the 21 keypoints, localize the them in the first two coordinate systems. Because the hand center is usually in motion and the camera is static, the trajectories in the camera coordinate system, instead of the hand world coordinate system, could be used to calculate the

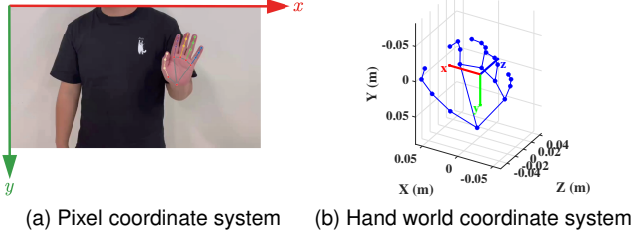


Fig. 3. Illustration of three coordinate systems.

Doppler frequencies. Thus, the coordinates of hand keypoints  $\mathbf{p}_i(t)$ ,  $i = 1, 2, \dots, 21$ , transmitter  $\mathbf{p}_t$  and receiver  $\mathbf{p}_r$ , defined in the previous section should be measured in the camera coordinate system. The above three coordinate systems and their transformation are illustrated in Fig. 3.

Define the coordinates of the  $i$ -th keypoint ( $i = 1, 2, \dots, 21$ ) in the pixel, hand world and camera coordinate systems as  $(u_i, v_i)$ ,  $(x_i^w, y_i^w, z_i^w)$ , and  $(x_i, y_i, z_i)$ , respectively, where the snapshot index  $t$  is ignored in this section for the simplicity of elaboration. Let  $f$  be the focal length in the unit of pixels,  $(c_x, c_y)$  be the coordinates of image center in the pixel coordinate system, we define the camera intrinsic matrix  $\mathbf{A}$  as

$$\mathbf{A} = \begin{bmatrix} f & 0 & c_x \\ 0 & f & c_y \\ 0 & 0 & 1 \end{bmatrix}. \quad (12)$$

Hence, the relation between the 2D pixel and 3D camera coordinate systems can be expressed as

$$z_i[u_i \ v_i \ 1]^T = \mathbf{A}[x_i \ y_i \ z_i]^T. \quad (13)$$

Let  $\mathbf{R} \in \mathbb{R}^{3 \times 3}$  and  $\mathbf{t}$  be the rotation matrix and translation vector from hand world coordinate system to camera coordinate system, we define the camera extrinsic matrix  $\mathbf{T}$  and perspective projection matrix  $\mathbf{\Pi}$  as follows:

$$\mathbf{T} = \begin{bmatrix} \mathbf{R} & \mathbf{t} \\ \mathbf{0}_{1 \times 3} & 1 \end{bmatrix}, \quad (14)$$

$$\mathbf{\Pi} = [\mathbf{I}_{3 \times 3} \ \mathbf{1}_{3 \times 1}], \quad (15)$$

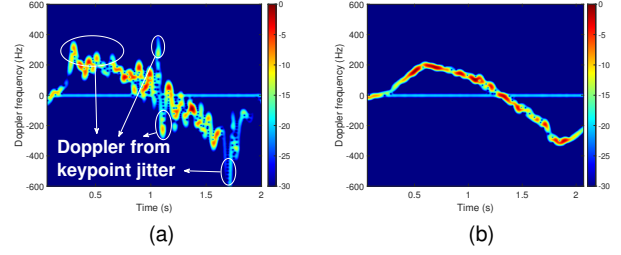


Fig. 4. Comparison of simulated spectrograms via CASTER (a) before keypoint smoothing, (b) after keypoint smoothing.

where  $\mathbf{I}_{3 \times 3}$  denotes a  $3 \times 3$  identity matrix,  $\mathbf{0}_{1 \times 3}$  and  $\mathbf{1}_{3 \times 1}$  are the three-dimensional row and column vectors with all 0 and 1 entries respectively. According to [12], the relations between the hand world and camera coordinate systems are given by

$$[x_i \ y_i \ z_i \ 1]^T = \mathbf{T}[x_i^w \ y_i^w \ z_i^w \ 1]^T. \quad (16)$$

As a result, the relation between the hand world and the pixel coordinate system could be described as

$$z_i[u_i \ v_i \ 1]^T = \mathbf{A}\mathbf{\Pi}\mathbf{T}[x_i^w \ y_i^w \ z_i^w \ 1]^T. \quad (17)$$

For the elaboration convenience, we denote the projection from the hand world coordinate system to the pixel coordinate system as the following function  $\mathcal{P}$ :

$$\begin{aligned} [u_i \ v_i]^T &= \mathcal{P}([x_i^w \ y_i^w \ z_i^w]^T, \mathbf{R}, \mathbf{t}, \mathbf{A}) \\ &= \frac{1}{z_i} [\mathbf{I}_{2 \times 2} \ \mathbf{0}_{2 \times 1}] \mathbf{A} (\underbrace{\mathbf{R}[x_i^w \ y_i^w \ z_i^w]^T + \mathbf{t}}_{=[x_i \ y_i \ z_i]^T}). \end{aligned} \quad (18)$$

The *Mediapipe* could provide the coordinates  $(u_i, v_i)$  and  $(x_i^w, y_i^w, z_i^w)$  of all the keypoints ( $i = 1, 2, \dots, 21$ ) in each video frame. Hence, their coordinates in the camera coordinate system can be calculated with the knowledge of the rotation matrix  $\mathbf{R}$  and translation vector  $\mathbf{t}$ .

In fact, the parameters in the camera intrinsic matrix  $\mathbf{A}$  can be measured in advanced, the rotation matrix  $\mathbf{R}$  and translation vector  $\mathbf{t}$  can be estimated via (18) for  $i = 1, 2, \dots, 21$ . Particularly, Given the coordinates of the 21 keypoints in the pixel and hand world coordinate systems, the detection of the rotation matrix  $\mathbf{R}$  and translation vector  $\mathbf{t}$  can be formulated as follows.

$$\begin{aligned} \min_{\mathbf{R}, \mathbf{t}} \quad & \sum_{i=1}^{21} |(u_i, v_i) - \mathcal{P}([x_i^w \ y_i^w \ z_i^w]^T, \mathbf{R}, \mathbf{t}, \mathbf{A})|^2, \\ \text{s.t.} \quad & \mathbf{R}(\mathbf{R})^T = \mathbf{I}_{3 \times 3}, \det(\mathbf{R}) = 1. \end{aligned} \quad (19)$$

The above problem is referred to as the Perspective-n-Point (PnP) problem [12]. It can be solved via the *cv2.solvePnP* function from the popular computer vision library *OpenCV* [13], where the Levenberg-Marquardt optimization method [14] is adopted.

### B. Motion Smoothing and Snapshot Interpolation

Because of the errors of keypoint detection with *Mediapipe*, there might be fake hops or jitters in the detected trajectories of keypoints, which do not exist actually. This will lead to the false alarm of high Doppler frequencies (as depicted in Fig. 4). In order to generate high-fidelity dataset for gesture classification model training, a low-pass filter, namely one-euro filter [15], is proposed to smooth both trajectories and velocities, followed by snapshot interpolation between neighboring video frames.

Let  $\mathbf{q}_{i,k} = [x_{i,k} \ y_{i,k} \ z_{i,k}]^T$  and  $\hat{\mathbf{q}}_{i,k} = [\hat{x}_{i,k} \ \hat{y}_{i,k} \ \hat{z}_{i,k}]^T$  be the positions of the  $i$ -th keypoint in the  $k$ -th frame before and after the low-pass filtering respectively,  $\dot{\mathbf{q}}_{i,k} = [\dot{x}_{i,k} \ \dot{y}_{i,k} \ \dot{z}_{i,k}]^T$  and  $\hat{\dot{\mathbf{q}}}_{i,k} = [\hat{\dot{x}}_{i,k} \ \hat{\dot{y}}_{i,k} \ \hat{\dot{z}}_{i,k}]^T$  be the estimated velocities of the  $i$ -th keypoint in the  $k$ -th frame before and after the low-pass filtering respectively. Initializing  $\hat{\dot{\mathbf{q}}}_{i,1}$  with  $\mathbf{q}_{i,1}$ , the trajectory smoothing for the  $i$ -th keypoint in the  $k$ -th frame is given by

$$\hat{o}_{i,k} = \alpha_{i,k} o_{i,k} + (1 - \alpha_{i,k}) \hat{o}_{i,k-1}, \quad \forall i, k \geq 2 \quad (20)$$

where the notation  $o$  represents the dimensions of  $x$ ,  $y$  and  $z$ , and

$$\alpha_{i,k} = \frac{1}{1 + \frac{1}{2\pi \Delta t_v (f_{c_{\min}} + \beta |\hat{o}_{i,k}|)}}$$

is the smoothing factor,  $\Delta t_v$  is the video frame interval,  $f_{c_{\min}}$  is the minimum cutoff frequency,  $\beta$  is the speed coefficient of update. Moreover, the velocity in the above equation can be calculated as

$$\hat{o}_{i,k} = \gamma \dot{o}_{i,k} + (1 - \gamma) \hat{o}_{i,k-1}, \quad \forall i, k \geq 2 \quad (21)$$

where  $\dot{o}_{i,k} = (o_{i,k} - \hat{o}_{i,k-1}) / \Delta t_v$ ,  $\hat{o}_{i,1}$  is initialized with 0,  $\gamma$  is the fixed smoothing factor.

Finally, we adopt the cubic spline interpolation method [16] to insert  $\Delta t_v / \Delta t_s - 1$  positions of the  $i$ -th keypoint ( $\forall i$ ) between every two neighboring frames (say  $\hat{\mathbf{q}}_{i,k}$  and  $\hat{\mathbf{q}}_{i,k+1}$ ,  $\forall k$ ), and denote the position of the  $i$ -th keypoint in the  $t$ -th snapshot as  $\mathbf{p}_i(t)$ .

### V. EVALUATION OF CASTER SIMULATOR

In this section, the high fidelity of the CASTER simulator in the applications of gesture recognition is demonstrated. Specifically, the generation of gesture datasets via CASTER simulator and real measurement is first elaborated. Then, the classification performance via the above two datasets is discussed.

#### A. Simulation and Experiment Datasets

In order to verify the quality of dataset generated by CASTER simulator, 300 clips of videos on 3 gestures, including pushing and pulling, beckoning, and rubbing fingers, were recorded using a normal monocular camera at a rate of 30 frame per second (fps). Thus, 100 sequences of channel impulse responses for each gesture are obtained via the proposed CASTER simulator with a sampling rate of 2000 snapshots per second. Then, one spectrogram, illustrating the

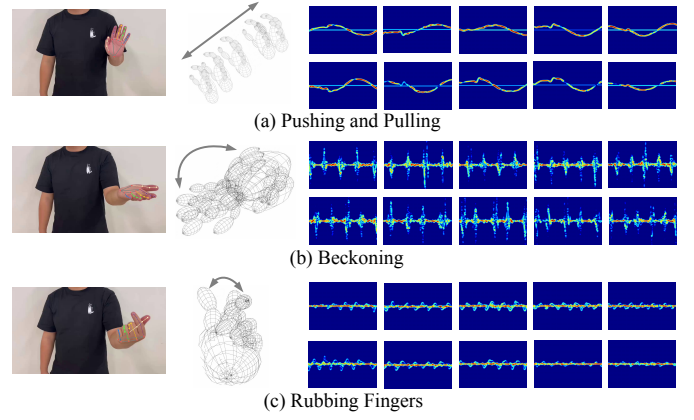


Fig. 5. Illustration of the simulated dataset from CASTER, where some examples of spectrogram are plotted.

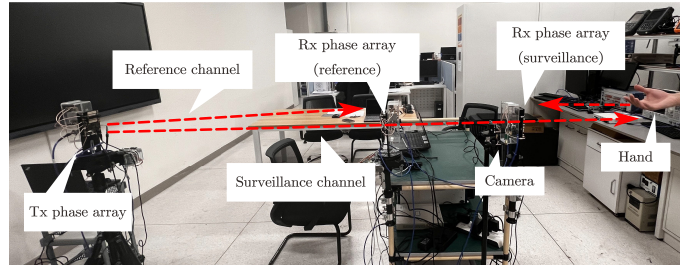


Fig. 6. Facilities and scenario of experiment.

Doppler frequency versus time, is calculated for each video clip (each sequence of channel impulse responses) by applying the short time Fourier transform (STFT) with a window of 0.125 seconds (250 snapshots). As a result, a simulated dataset of 300 spectrograms for the recognition of three gestures is obtained as illustrated in Fig. 5.

In order to measure the real Doppler spectrum of gestures, an integrated passive sensing and communication system working on millimeter wave (mmWave) band is developed as in our previous work [17]. As illustrated in Fig. 6, at the transmitter, an NI USRP-2954R [18] is utilized to generate an intermediate frequency (IF) signal at 500 MHz, which is subsequently up-converted to 60 GHz and transmitted using a Sivers 60 GHz phased array [19]. At the receiver, two phased arrays are connected to a single USRP device to receive signals from the reference and surveillance channels, respectively. The transmit mmWave signal is modulated via the orthogonal frequency-division multiplexing (OFDM). The carrier frequency is 60.48 GHz and signal bandwidth is 5 MHz.

In the experiment, the locations of transmitter and receiver are consistent with those in the simulator. 100 trials are measured for each gesture via the passive sensing system. Following the signal processing in [17], the spectrogram of hand gestures can be computed through the cross-ambiguity function. As a result, an experiment dataset with 100 spectrograms per gesture is obtained.



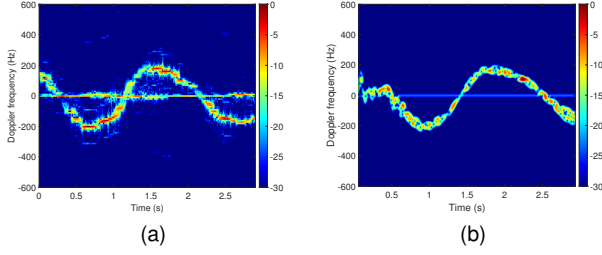


Fig. 7. Spectrograms of the gesture of pushing and pulling: (a) experiment measurement; (b) CASTER simulator.

## B. Performance of Gesture Recognition

First of all, it can be observed from Fig. 7 that the spectrograms from real experiment and CASTER simulator exhibit similar time-Doppler patterns. To further demonstrate the high fidelity of the proposed simulator in the applications of gesture recognition, the following six training and testing schemes are adopted with the same image classification model named ResNet18 [20]:

- **Scheme 1:** The training set consists of 60 simulated spectrograms for each gesture, and the test set consists of 40 measured ones for each gesture;
- **Scheme 2:** The training set consists of 50 simulated spectrograms and 10 measured ones for each gesture, and the test set consists of 40 measured ones for each gesture;
- **Scheme 3:** The training set consists of 40 simulated spectrograms and 20 measured ones for each gesture, and the test set consists of 40 measured ones for each gesture;
- **Scheme 4:** The training set consists of 30 simulated spectrograms and 30 measured ones for each gesture, and the test set consists of 40 measured ones for each gesture;
- **Scheme 5:** The training set consists of 60 measured spectrograms for each gesture, and the test set consists of 40 measured ones for each gesture;
- **Scheme 6:** The training set consists of 60 simulated spectrograms for each gesture, and the test set consists of 40 simulated ones for each gesture.

The overall results of the gesture recognition are shown in Fig. 8, and the confusion charts of the 6 schemes are shown in Fig. 9 respectively. It can be observed that an accuracy of 90.8% (Scheme 1) can be achieved if the simulated dataset is used for training and the experimental dataset is used for testing. Thus, CASTER simulator could generate channel impulse responses with sufficient quality for the applications of wireless gesture recognition. On the other hand, there is still 10% performance loss compared with the Scheme 5 and 6, indicating that the difference between simulated and experimental datasets is not negligible. One method to mitigate such difference is to mix some experimental samples into the simulated dataset. It can be observed from the results of Scheme 2, 3, 4 that mixing some experimental samples could significantly improve the testing accuracy.

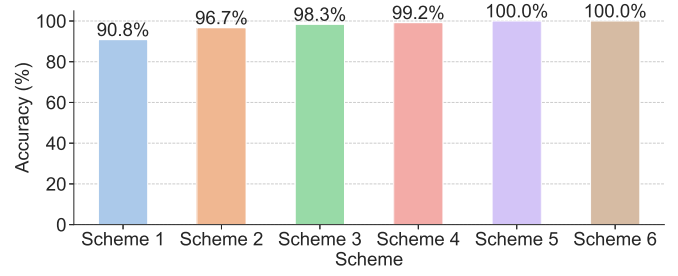


Fig. 8. Gesture recognition accuracy of the 6 training and testing schemes.

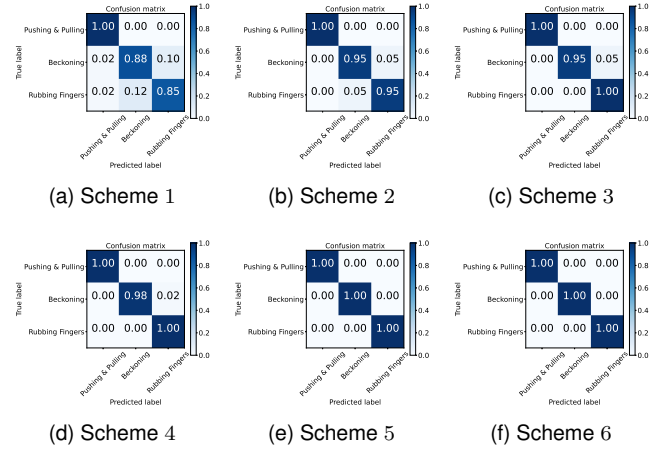


Fig. 9. Confusion charts of the 6 training and testing schemes.

## VI. CONCLUSION

In this paper, a computer-vision assisted wireless channel simulator, namely CASTER simulator, is proposed to generate high-fidelity dataset for hand gesture recognition. In the simulator, the target hand is modelled by 21 ellipsoid primitives, and the ray-tracing method is adopted to calculate the channel impulse responses. Moreover, a video gesture catcher is proposed to capture real motion data of gestures. In the experiments, both real dataset via experiment and simulated dataset via CASTER simulator are obtained. A high accuracy of 90.8% can be achieved in simulation-to-reality inference, i.e., using simulated and experimental datasets in model training and inference respectively.

## REFERENCES

- [1] R. Du *et al.*, "An overview on ieee 802.11 bf: Wlan sensing," *arXiv preprint arXiv:2207.04859*, 2022.
- [2] M. Zhang *et al.*, "Channel models for WLAN sensing systems," *IEEE 802.11 Documents*, Sep. 2021.
- [3] G. Li *et al.*, "Wireless sensing with deep spectrogram network and primitive based autoregressive hybrid channel model," in *IEEE 2021 SPAWC*, 2021, pp. 481–485.
- [4] G. Li *et al.*, "Integrated sensing and communication from learning perspective: An sdp3 approach," *IEEE Internet Things J.*, 2023.
- [5] "Wigig tools," [Online]. Available: <https://github.com/wigig-tools>
- [6] S. Vishwakarma *et al.*, "Simhumalator: An open-source end-to-end radar simulator for human activity recognition," *IEEE Aerosp. Electron. Syst. Mag.*, vol. 37, no. 3, pp. 6–22, 2021.
- [7] B. Erol *et al.*, "Simulation of human micro-doppler signatures with kinect sensor," in *2014 IEEE Radar Conference*, 2014, pp. 0863–0868.

- [8] R. Boulic *et al.*, “A global human walking model with real-time kinematic personification,” *Visual Comput.*, vol. 6, pp. 344–358, 1990.
- [9] E. F. Knott *et al.*, *Radar cross section*. SciTech Publishing, 2004.
- [10] K. D. Trott, “Stationary phase derivation for rcs of an ellipsoid,” *IEEE Antennas Wireless Propag. Lett.*, vol. 6, pp. 240–243, 2007.
- [11] F. Zhang *et al.*, “Mediapipe hands: On-device real-time hand tracking,” *arXiv preprint arXiv:2006.10214*, 2020.
- [12] E. Marchand *et al.*, “Pose Estimation for Augmented Reality: A Hands-On Survey,” *IEEE Trans. Vis. Comput. Graphics*, vol. 22, no. 12, pp. 2633 – 2651, Dec. 2016.
- [13] “Opencv: Perspective-n-point (pnp) pose computation.” [Online]. Available: [https://docs.opencv.org/4.x/d5/d1f/calib3d\\_solvePnP.html](https://docs.opencv.org/4.x/d5/d1f/calib3d_solvePnP.html)
- [14] K. Levenberg, “A method for the solution of certain non-linear problems in least squares,” *Quarterly of applied mathematics*, vol. 2, no. 2, pp. 164–168, 1944.
- [15] G. Casiez *et al.*, “1€ filter: a simple speed-based low-pass filter for noisy input in interactive systems,” in *CHI '12*, 2012, pp. 2527–2530.
- [16] C. De Boor *et al.*, *A practical guide to splines*. springer-verlag New York, 1978, vol. 27.
- [17] J. Li *et al.*, “Passive motion detection via mmwave communication system,” in *VTC 2022-Spring*. IEEE, 2022, pp. 1–6.
- [18] National Instruments. Usrp-2954. [Online]. Available: <https://www.ni.com/en-us/shop/model/usrp-2954.html>
- [19] Sivers IMA. Evk 06002/00. [Online]. Available: <https://www.siversima.com/product/evk-06002-00/>
- [20] K. He *et al.*, “Deep residual learning for image recognition,” in *CVPR '16*, 2016, pp. 770–778.